Effects of Nano $LiTaO_3$ Crystallization on Dielectric and Optical Properties in Er^{3+}-doped Li_2O-Ta_2O_5-SiO_2-Al_2O_3 Glasses

Anal Tarafder, Kalyandurg Annapurna, Reenamoni Saikia Chaliha, and Basudeb Karmakar*
Glass Science and Technology Section, Glass Division, Central Glass and Ceramic Research Institute, Council of Scientific and Industrial Research (CSIR),
196, Raja S.C. Mullick Road, Kolkata 700 032, India

Vidya Sagar Tiwari, and Pradeep Kumar Gupta
Laser Materials Development and Devices Division,
Raja Ramanna Center for Advanced Technology, Indore 452 013, India

Abstract

The precursor glass of $LiTaO_3$ nanocrystals was prepared in a new Er^{3+}-doped Li_2O-Ta_2O_5-SiO_2-Al_2O_3 (LTSA) system by the melt-quench technique. They were isothermally crystallized at 680°C for 3-100 h to obtain nanostructured glass-ceramics. The X-ray diffraction (XRD) and transmission electron microscopy (TEM) confirm nanocrystallization of $LiTaO_3$ (16-34 nm) yielding transparent glass-ceramics. A steep rise in dielectric constant with heat-treatment time is attributed to ferroelectric $LiTaO_3$ crystallization. Photoluminescence spectra exhibit the $^4I_{13/2} \rightarrow {}^4I_{15/2}$ emission transition of Er^{3+} ions at 1570 nm when excited at 984 nm. Its intensity and lifetime decrease with increase in heat-treatment time due to concentration quenching effect.

---

* *Corresponding author. Tel.: +91 33 2473 3469; Fax: +91 33 2473 0957.*

E-mail address: basudebk@cgcri.res.in (B. Karmakar).

Introduction

Among the lead-free ferroelectric materials in the $A^{1+}B^{5+}O_3$ type perovskite family, the rhombohedral lithium tantalate ($LiTaO_3$, LT) single crystal with crystal symmetry class *R3c* (unit cell dimensions: a = 5.1530 Å and c = 13.755 Å) is one of the most important due to its large nonlinear coefficient (d_{33} = 13.8 pm/V at 1064 nm) and large second harmonic generation (SHG) coefficient ($d_{33}^{2w} = 40.0$ at 1060 nm).[1-3] Its single crystal shows unique piezoelectric, acousto-optic, electro-optic and non-linear optical (NLO) properties combined with good mechanical and chemical stability.[4-7] Rare-earth (RE) doped glasses are of great interest on account of their optical and fluorescence properties. The combination of high optical transparency and good fluorescence characteristics of a low phonon energy environment is needed for RE upconversion materials which is important for the development of fiber lasers and efficient amplifiers. Rare-earth doped transparent nano $LiTaO_3$ crystal containing glass-ceramics, in which rare-earth ions selectively incorporated into the $LiTaO_3$ nanocrystals embedded in an oxide glassy matrix, can offer excellent luminescent properties due to the low phonon energy environment of $LiTaO_3$ nanocrystals for luminescent ions, and good mechanical and chemical properties of oxide glassy matrix. This ability, combined with inherent nonlinear optical (NLO) properties of ferroelectric crystals, could offer a possibility to design self frequency doubling laser sources. Hence, this new material has attracted great attention in the continuous research for the novel optoelectronic devices.[8-12] The dielectric properties of the $LiTaO_3$ single crystal[13] and Ag(Nb, Ta)O_3 ceramics[14] have been studied to explore the functional properties of these materials. However, work performed on nano $LiTaO_3$ crystal containing glass-matrix materials is very rare due to difficulties in the preparation of transparent precursor glass and glass-ceramics, and the requirement of high temperature (about 1600^{o}C) for its precursor glass melting.[15] Probably for

these reasons, effects of nano $LiTaO_3$ crystallization on dielectric and fluorescence properties in Er^{3+}-doped Li_2O-Ta_2O_5-SiO_2-Al_2O_3 (LTSA) glasses have not been reported so far. This fact has motivated us to explore this gap.

Glass materials are attractive hosts for rare-earth ions (RE^{3+}) because planar waveguides and optical fibers can be fabricated easily with them compared to crystalline materials. Er^{3+} is one of the most widely studied luminescent ions, and Er^{3+} doped crystalline, glass and ceramics have been applied in many fields. One main NIR emission from Er^{3+} ions is at 1550 nm and located in the 'eye-safe' spectral region. It (Er^{3+}) has been extensively used as active ion for the optical telecommunication systems, not only for the optical amplification at the third communication window, but also for the upconversion lasers of visible green emission at 550 nm.[16-21] Moreover, the Er^{3+} ion has a number of strong absorption bands where the effective pumping sources are available. In the near infrared region, for Er^{3+} transition $^4I_{15/2} \rightarrow {}^4I_{11/2}$ (at about 980 nm) can be efficiently excited to obtain down and upconversion emissions.[22, 23] Hence, it will be interesting to investigate the evolution of spectroscopic properties of doped Er^{3+} ions in $LiTaO_3$ nanocrystals in LTSA glass matrix.

In view of above, in the present work, we focus our systematic analysis on the preparation of precursor glass and subsequently crystallization of nano $LiTaO_3$ crystal in Er^{3+} ion doped LTSA glasses. The crystallization process has been studied by differential thermal analysis (DTA), X-ray diffraction (XRD), field emission scanning electron microscopy (FESEM), transmission electron microscopy (TEM), Fourier transform infrared reflection spectra (FT-IRRS), UV-excited (378 nm) visible fluorescence and NIR-excited (984 nm) NIR fluorescence analyses, excited state lifetime analysis and dielectric constant measurement. In short, the aim of this work

is to develop a promising transparent nano glass-ceramics for new fiber laser and efficient amplifiers.

Experimental Procedure

Precursor Glass Preparation

The precursor glass having molar composition $25.53Li_2O$-$21.53Ta_2O_5$-$35.29SiO_2$-$17.65Al_2O_3$ doped with Er_2O_3 (0.2 mol% in excess) was prepared from pure chemicals such as Li_2CO_3 (GR, 99%, Loba Chemie), Ta_2O_5 (99.85%, Alfa Aesar), SiO_2 (99.8%, Sipur A1 Bremtheler Quartzitwerk), Al_2O_3 (99.8%, CT 1200 SG, Almatis), and Er_2O_3 (99.9%, Alfa Aesar) powders by conventional melt-quench technique. The well-mixed batch of about 200 g glass was melted in a platinum crucible in an electric furnace at 1600°C for 2h in air. The glass melt was poured onto a pre-heated iron mould. It was annealed at 600°C for 4 h to remove the internal stresses of the glass and then slowly cooled down (@ 1^oC/min) to room temperature. The as-prepared glass block was cut into desired dimensions and optically polished for ceramization and to perform different measurements.

Characterization

The density of precursor glass was measured using Archimedes principle using water as buoyancy liquid. The refractive indices of precursor glass (a) and representative glass-ceramics (d) were measured on a Metricon 2010/M Prism Coupler at different wavelength (λ = 473, 532, 633, 1064 and 1552 nm). Differential thermal analysis (DTA) of precursor glass powder was carried out up to 1000^oC at the rate of 10^oC/min with a SETARAM TG/DTA 92 instrument to ascertain the glass transition temperature (T_g) and the crystallization peak temperature (T_P). XRD data were recorded using a PANalytical X'Pert-PRO MPD diffractometer operating with

CuK_α = 1.5406 Å radiation to identify the developed crystalline phases. The data were collected in the 2θ range from 10^o to 80^o with a step size of 0.05^o.

A high resolution FE-SEM (Model: Gemini Zeiss Supra^{TM} 35 VP, Carl Zeiss) was used to observe the microstructure of freshly fractured surfaces of the heat-treated nano glass-ceramics after etching in 1% HF solution for 2 minutes and coated with a thin carbon film. The TEM images and selected area electron diffraction (SAED) of powdered glass-ceramic sample were obtained from FEI (Model: Tecnai G^2 30ST, FEI Company) instrument. The FTIR reflectance spectra of all Er^{3+}-doped glass and glass-ceramics were recorded using a FTIR spectrometer (Model: 1615, Perkin-Elmer) in the wavenumber range 400-2000 cm^{-1} with a spectral resolution of ±2 cm^{-1} and at 15^o angle of incidence. Optical absorption spectra were recorded on UV-Vis-NIR spectrophotometer (Model: Lambda 20, Perkin-Elmer) at room temperature to monitor the changes of the environmental structure of the Er^{3+} ions. The UV-Vis fluorescence emission and excitation spectra were measured on a fluorimeter (Model:Fluorolog-II, SPEX) with 150 W Xe lamp as a source of excitation. The NIR excited (984 nm) emission spectra were measured on NIR enhanced continuous bench top modular spectrofluorimeter (QuantaMaster, Photon Technology International) attached with gated Hamamatsu NIR PMT (P1.7R) as detector and Xe arc lamp as excitation source. The excited state lifetime was measured with the same instrument using a Xe flash lamp of 75 W. The dielectric constants of precursor glass and nano glass-ceramics were measured at room temperature using a Hioki LCR meter (Model: 3532-50 Hitester, Hioki) at 1 MHz frequency after coating the surfaces with a conductive silver paint followed by drying at 140^oC for 1h.

Results and Discussion

Thermal, Optical and other Physical Properties

In preliminary examination, it was observed that more quantity (>47.06 mol%) of Li_2O and Ta_2O_5 (i.e., Li_2O + Ta_2O_5) could not be incorporated in the glass matrix without sacrificing the transparency. For this reason, the particular composition of $25.53Li_2O$-$21.53Ta_2O_5$-$35.29SiO_2$-$17.65Al_2O_3$ (mol%), which yield transparent precursor glass was selected and doped with Er_2O_3 (0.2 mol% in excess) for this investigation. The DTA curve of the precursor glass is shown in Fig. 1. It exhibits an inflection in the temperature range 680-715^oC followed by an intense exothermic peaks at 820^oC (T_p) corresponding to the $LiTaO_3$ crystallization. The glass transition temperature (T_g) has been estimated to be 698^oC from the point of intersection of the tangents drawn at the slope change as is marked in Fig. 1.

The precursor glass is visually transparent, appearing pinkish due to Er^{3+} doping. The precursor glass samples were heat treated at 680^oC near glass transition temperature for 0, 3, 5, 10, 20, 50 and 100 h after nucleating at 650^oC for 2 h. The obtained samples were labeled as (a)-(g) (Fig. 2) respectively for convenience. The transparency of the precursor glass persists in heat-treated samples although the samples have been appeared gradually translucent due to devitrification with progress of heat-treatment duration. This is clearly seen from Fig. 2. From the measured glass density (ρ) and refractive index (n_D) at wavelength λ_D = 589.2 nm, other related optical properties have been determined using relevant expressions[24] and the results are presented in Table I. Fig. 3 (Cauchy fitting based on refractive index measurement at five different wavelengths, see Section 2) shows the dependences of the refractive index on the wavelength for precursor glass (a) and the 10 h heat-treated glass-ceramics (d) sample. In general, refractive index decreases with increasing wavelength due to dispersion. This trend is

observed in both the samples. In addition to this, the refractive index of the glass-ceramic sample (d) has increased in comparison with precursor glass (a) that can be seen in Fig.3. From Table I, it is clear that the LTSA glass under study has high values of refractive index and density. The large refractive indices of these glasses are due to high ionic refraction (23.4) of Ta^{5+} ions[25] having empty or unfilled d-orbital (outer electronic configuration: $5d^0 6s^0$) which contributes strongly to the linear and nonlinear polarizability.[26] Where as high density results from its large packing effect in the glass matrix.[27] For the same reason, this glass possesses a high value of molar refractivity (R_M = 12.72 cm^3) and electronic polarizability (α=1.93 x 10^{-21} cm^3). Due to formation of high refractive index $LiTaO_3$ (RI=2.1834 at 600 nm[28]), the heat-treated sample exhibit higher refractive indices as shown in Fig. 3, curve-d.

X-ray Diffraction Analysis

The X-ray diffractograms of precursor glass and cerammed nano glass-ceramics are shown in Fig. 4. The XRD pattern of the precursor glass exhibits broad humps characterizing its amorphous nature. With progression of heat-treatment, several diffraction peaks appeared which are attributed to rhombohedral $LiTaO_3$ (JCPDS Card File No. 29-0836) except a few diffraction peak around 2θ = 23.03°, 25.37°, 44.45° and 47.11° which are due to the formation of β-spodumene ($LiAlSi_2O_6$) crystal phase (JCPDS Card File No. 35-0797) in minor quantity. Hsu and Speyer[29] have reported that the Ta_2O_5 acts as a nucleating agent in the Li_2O-Al_2O_3-SiO_2 glass system which exhibits β-quartz solid solution (*ss*) crystallization, where β-spodumene is one of them, peak in the temperature range 800-900°C particularly at higher concentration of Ta_2O_5. In the present case, the small crystallization peak (minor) of β-spodumene in the DTA thermogram might have merged with the large crystallization peak (major) of the $LiTaO_3$ at

820°C. This could be the reason of exhibiting two crystal phases in the XRD patterns although DTA curve shows only single sharp crystallization peak around 820°C. It is clearly evidenced from the XRD analysis that the peak of $LiAlSi_2O_6$ ($2\theta = 25.30^o$) is more prominent in sample d with 5 h heat-treatment and it got diminished with respect to $LiTaO_3$ phase in samples (d)-(g), indicating the stabilization of $LiTaO_3$ nanocrystallites. The XRD pattern of nano glass-ceramics (b) differs due to its phase-separated glassy nature and having different structure than the precursor glass (a) and 5 h heat-treated nano glass-ceramics (c). From the full width at half maximum (FWHM) of the intense diffraction peak (012) of $LiTaO_3$, the average crystallite size (diameter, d) is calculated by using the Scherrer's formula[30]

$$d = 0.9\lambda / \beta \cos\theta \qquad (1)$$

where λ is the wavelength of X-ray radiation (CuK_α = 1.5406Å), β is the full width at half maximum (FWHM) of the peak at 2θ.

The diameter of the $LiTaO_3$ crystallites is plotted as a function of heat-treatment time in Fig. 5. The average crystallite size increases with heat-treatment duration and found to vary from 16 to 34 nm for samples (b)-(g). The error of estimation is ±2%.

FESEM and TEM Image Analyses

The morphology and the size of $LiTaO_3$ nanocrystallites in nano glass-ceramics have been examined by FESEM and TEM image analyses. FESEM images of the fractured surface of samples (c) and (f) have been presented in Figs. 6(a) and (b) respectively. From the FESEM micrographs, it is clearly observed that the glassy matrix of the heat-treated samples initially phase separated on nanometric scale followed by incipient precipitation of defined crystallites within the Li–Ta rich phase regions with increase in heat-treatment time. The droplets have

irregular shape and are spread out uniformly thought out the bulk glass matrix. The size of the droplets varies in the range 30-60 nm. The TEM bright field image, the corresponding selected area electron diffraction pattern and HRTEM of the 5 h heat-treated samples are shown in Figs. 7(a) and (b). From these images, it is observed that many spheroidal $LiTaO_3$ crystallites precipitated homogeneously from the glass matrix and homogeneously dispersed in the residual glass matrix. The crystallite size from TEM image of sample (c) is found to be around 20 nm. The presence of fine spherical rings around the central bright region in SAED pattern also discloses the existence of $LiTaO_3$ nanocrystallites in the glassy matrix. The d-spacing (3.74 Å) as obtained from Fig. 7(b) matches well with JCPDS card file no. 29-0836, which again confirms the formation of $LiTaO_3$ crystallites in the nano glass-ceramics.

Fourier Transform Infrared Reflectance Spectroscopy

The FTIR reflectance spectra of the precursor glass and nano glass-ceramics in the wavenumber range 400-2000 cm^{-1} are shown in Fig. 8. It is seen from this figure that the precursor glass (curve-a) exhibits two broad reflection bands centered around 960 and 610 cm^{-1} as a result of wider distribution of silicon and tantalate structural units respectively. This is an indication of the structural disorder existing in the amorphous network with the presence of SiO_4 tetrahedra and TaO_6 octahedra having different number of non-bridging oxygen. The broad reflectance band at 960 cm^{-1} is attributed due to the overlapping of Si-O and Ta-O stretching vibrations. In spite of the transparent nature of the heat-treated samples, their FT-IR reflectance spectra (curves b and g) reveal narrowing of the main two reflection bands with additional feature arising at 735 cm^{-1} in comparison to the as prepared glass. In the FT-IRR spectra, the stretching modes of the Si-O-Si bonds of the SiO_4 tetrahedra with nonbridging oxygen (NBO)

atoms are active around 1000 cm^{-1} (high energy side) and the stretching modes of the Ta-O bonds in the TaO_6 octahedra occur in the 600-650 cm^{-1} range (low energy side) due to higher atomic weight of Ta. The variation of Si-O (998 cm^{-1}) and Ta-O (602 cm^{-1}) stretching vibration bands intensities with heat-treatment time is shown in the inset of Fig. 8. It is seen that with progression of heat-treatment the bands intensities increases rapidly initially and then become almost saturated after a certain time of heat-treatment (10 h). The appearance of a low intensity band upon heat-treatment at 735 cm^{-1} related to the stretching mode of Al-O bond of AlO_4 tetrahedra of spodumene.[31] The prominent band occurred at 602 cm^{-1} corresponds to the stretching mode of O-Ta bond of TaO_6 octahedral units of lithium tantalate.[32, 33] The reflection band centered at 602 cm^{-1} is assigned as $LiTaO_3$ crystal formation and the reflection band centered at 998 cm^{-1} is assigned to Si-O stretching vibration of residual glass and spodumene crystal. Two bands generated at 998 and 602 cm^{-1} in the FTIR spectrum (Fig. 8, curve-b) after 3 h heat-treatment at 680^{o}C give the clear evidence of phase separation of precursor glass into Si-rich and Li-rich phases respectively, which exhibits very feeble sign of crystallization in the XRD pattern (Fig. 4, curve b). The gradual increase of relative intensity of band at 602 cm^{-1} clearly indicates formation of $LiTaO_3$ crystal with the increase of heat treatment time. Thus from the investigations carried out on the measured FT-IR reflectance spectra of Er^{3+}-doped LTSA precursor glass and nano glass-ceramics as described above provide the information of crystallization with initial phase separation followed by advancement of mainly $LiTaO_3$ crystal formation in the glass matrix. The results of the FT-IRRS are in good agreement with that of XRD, FE-SEM and TEM studies. A similar observation has also been reported by Ito, et al[15]

Dielectric Constant (ε_r)

Glass and glass-ceramics have certain advantages as dielectric materials because of their high dielectric strength. But, the disadvantages of glass are a low permittivity (ε_r = 4-15) and a low thermal conductivity (about 1 W $m^{-1}K^{-1}$).[34] In the present study, the precursor Er^{3+}-doped LTSA precursor glass has exhibited relatively higher value (20.5) of dielectric constant (ε_r) than the common vitreous silica (3.8) or borosilicate glasses (4.1-4.9) or soda-lime silicate (7.2)[35] due to high ionic refraction of Ta^{5+} ions (23.4).[25] This is due to its empty d-orbital ($5d^o6s^o$) which contributes very strongly to its high polarizability[26, 36] Its magnitudes show a sharp increase with increase in heat-treatment duration up to 5 h and thereafter it maintained saturation with a small decrease for any further heat treatment time as shown in Fig.9. This suggests that, at the initial stages of heat treatment (3 h), separation of silica rich phase and Li–Ta enriched phases takes place and with the further heat-treatment, incipient precipitation of $LiTaO_3$ crystalline phase of high dielectric constant (ε_r = 52)[3] and spontaneous polarization (P_s = 0.50 C/m^2)[1] occurs gradually which becomes well defined at 5 h and attains the maximum volume fraction of the crystalline phase. This is clearly evidenced from the observation of changes in XRD curves patterns as shown in the (b) and (c) of Fig. 4. Thus accumulation of Li^+ ions in the phase-separated glass matrix initially could cause a slight increase of dielectric constant and with further heat treatment time due to formation of stable $LiTaO_3$ ferroelectric crystals remarkably increase the dielectric constant reaching the highest value for 5 h heat treated sample and then maintain almost same on further course of heat-treatment. FESEM image analyses attribute to the presence of 0.10 and 0.13 volume fraction of glassy phase in nano glass ceramics (c) and (f) respectively. The remaining volume fractions 0.90 and 0.87 are due to the $LiTaO_3$ crystalline phase in respective nano glass-ceramics. Hence, it is clear that the variation in the dielectric

constant (ε_r) values among the heat-treated nano glass-ceramics are mostly due to volume fraction of crystal phases contained and also the distribution of the $LiTaO_3$ phase in the microstructure.[37] Based on this result again ascertains the observations made from XRD and TEM analyses on the nanocrysatallization of $LiTaO_3$ phase in the glass matrix.

UV-Vis-NIR Absorption Spectra

The ultraviolet-visible-near infrared (UV-Vis-NIR) absorption spectra of the Er^{3+}-doped precursor glass (a), 3 and 5 h heat treated nano glass-ceramics (samples b and c respectively) is shown in Fig. 10. The absorption peaks observed in the precursor glass spectrum corresponds to the transitions from ground state $^4I_{15/2}$ to the excited states of Er^{3+} and which are assigned, according to Carnall's convention,[38] as $^4G_{11/2}$, $^2H_{9/2}$, $^4F_{5/2}$, $^4F_{7/2}$, $^2H_{11/2}$, $^4S_{3/2}$, $^4F_{9/2}$, $^4I_{9/2}$, $^4I_{11/2}$ respectively. The changes of the Er^{3+} site environmental structure as the result of host transformation from glass to nano glass-ceramics causes the difference in optical spectroscopy. The most evident difference due to the heat-treatment is that the ultraviolet absorption edge (the inner illustration) red shifted and absorption spectra base line of nano glass-ceramics uplifted in comparison to precursor glass base line. This uplifting can be attributed to scattering of short wavelength light by the crystals[39, 40] or may be due to the large difference in refractive index of crystalline phase (RI of $LiTaO_3$ is 2.1834 at 600 nm[28] with that of residual glassy matrix (RI=1.7819 at 656.3 nm, see Table I)). Since the crystallites (16-34 nm) are smaller than the visible wavelength, a Rayleigh scattering model should be applicable.[41] According to this model, the scattering loss, τ is given by

$$\tau = \frac{32\pi^4 d^3 (n\Delta n)^2}{3\lambda^4} NV \qquad (2)$$

where *d* is the particle diameter, λ the wavelength of light, *n* the refractive index, *N* the number density of particles, and *V* the volume of the particle. With progression of heat-treatment, the number and sizes of nanocrystallites developed in the glassy matrix increase and hence the scattering centre and scattering loss increase that corresponds to a decrease in the visible transparency of the nano glass-ceramics samples. There is no significant difference in the shapes of absorption bands for glass and crystallized sample. During heat-treatment of the glasses, the hypersensitive transition (obeying selection rule: $\Delta J \leq 2$, $\Delta L \leq 2$ and $\Delta S = 0$ with large value, 0.713 of squared reduced matrix element, $|U^{(2)}|^2$) of Er^{3+} ion, $^4I_{15/2} \leftrightarrow {}^2H_{11/2}$ lying around 520 nm has been selected to understand the environment change closely around the rare-earth ion which is shown in Fig. 10 (inset). The absorption peaks is progressively sharpened in 5 h heat-treated sample due to the line narrowing associated to the glass-crystal transformation around the rare-earth ion[42] and the incorporation of Er^{3+} ions into $LiTaO_3$ crystallites during crystallization with negligible shift of the peak positions.

UV-Excited Visible Fluorescence

The visible fluorescence (λ_{ex} = 378 nm) spectra of samples are shown in Fig. 11 and the excitation spectra (λ_{em} = 549 nm) of precursor glass (a) and nano glass-ceramics (c) in the wavelength range 350-500 nm are shown in Fig. 12. The bands obtained from excitation spectra are assigned as $^4G_{11/2}$, (^2G, $^4F)_{9/2}$, $^4F_{5/2}$ and $^4F_{7/}2$.[38] From the excitation spectrum, peak wavelength λ= 378 nm of intense transition $^4I_{15/2} \rightarrow {}^4G_{11/2}$ has been selected to record the photoluminescence spectra of Er^{3+}-doped glass and nano glass-ceramics. All the luminescent spectra show a bright green emission at 549 nm due to transition $^4S_{3/2} \rightarrow {}^4I_{15/2}$ and with relatively

low intense emissions at 529 nm ($^2H_{11/2} \rightarrow {}^4I_{15/2}$) and 669 nm ($^4F_{3/2} \rightarrow {}^4I_{9/2}$). It is seen that the emission bands show sharp structure with progress of heat-treatment duration. Moreover, the relative intensity ratio of the 550 nm band to the 530 nm band increases with the heat-treatment time. The increase of fluorescence intensity is due to an increase in the symmetry of ligand fields and decrease of covalency. All these facts confirm the incorporation of Er^{3+} ion into the $LiTaO_3$ crystals.

NIR-Excited NIR Fluorescence and Lifetime

The near-infrared fluorescence spectra (λ_{ex} = 984 nm) of the samples around 1570 nm are shown in Fig. 13. The emission band intensity around 1570 nm decreases with heat-treatment time. This decrease in emission intensity is due to the clustering of Er^{3+} ions which is extremely sensitive to concentration quenching.[43] Dejneka[44] has demonstrated in oxyfluoride glasses that clustering thereby quenching occurs when the Eu^{3+}-Eu^{3+} ionic separation is around 40 Å. In the present case, the Er^{3+}-Er^{3+} ionic separation (R_i) in the precursor glass is found to be about 27 Å which was calculated using the relation[45]:

$$R_i(\overset{o}{A}) = (1/N_{Er^{3+}})^{1/3} \qquad (3)$$

where $N_{Er}{}^{3+}$ is the Er^{3+} ion concentration as already provided in Table I. It is, therefore, seen that the Er^{3+}- Er^{3+} ionic separation (R_i) is in the quenching region. Theoretically, the rate of relaxation due to concentration quenching varies as R_i^{-6}.[45, 46] With the progression of heat-treatment, the $LiTaO_3$ crystal phase has been formed and the Er^{3+} ions partitioned into the residual glassy phase by reducing the inter-ionic separation less than 27 Å of precursor glasses. This fact results in reduction in fluorescence intensity (see curve-b, c and g, Fig. 13) due to concentration quenching. The emission bands become sharper and take shapes as in crystalline host with

progress of heat-treatment duration. The broad emission band of precursor glass around 1530 nm is resolved into two peaks with increase of heat-treatment time due to stark splitting. All these observations indicate that the Er^{3+} ions enter into the $LiTaO_3$ crystalline phase and therefore, environment around Er^{3+} ions is changed with progression of heat-treatment.

The room temperature fluorescence decay curves of the emission transition ($^4I_{13/2} \rightarrow {}^4I_{15/2}$) at 1570 nm with an excitation at 984 nm for Er^{3+} ions in as-prepared glass and nano glass-ceramics have been depicted in Fig. 14. The measured curves demonstrate a single exponential decay. The excited state lifetime (τ) for all has been estimated from these decay curves and the results of sample (a)-(c), (e) and (f) are shown in inset of Fig. 14. It is seen that the excited state ($^4I_{13/2}$) lifetime (τ) decreases with increase in heat-treatment duration. This result indicates that Er^{3+} ions under going clustering upon formation of nano glass-ceramics. This change in the heat treatment conditions leads to changes in the volume of crystallinity in the nano glass-ceramics and in the lifetime of the $^4I_{13/2}$ state due to the concentration quenching.[42, 47] Further investigations are in progress to examine the concentration effects and also the limiting concentration of the cluster formation in this host.

Conclusions

Transparent glass-ceramics containing nano $LiTaO_3$ crystals in the lithium aluminosilicate glass matrix were prepared and the formation of nano $LiTaO_3$ crystals has been confirmed by XRD, FT-IRR spectra, FESEM and TEM images. The nanocrystallite size of $LiTaO_3$ has been evaluated from XRD and found to vary in the range 16-34 nm. This evaluation correlates well with those obtained from TEM images. The increase of dielectric constant in comparison to precursor glass confirms the formation ferroelectric $LiTaO_3$ crystal of high dielectric constant (ε_r

= 52) in glassy matrix. The absorption spectra, UV-excited visible fluorescence and NIR-excited higher NIR fluorescence spectra of nano glass-ceramics demonstrate that the Er^{3+} ion has entered into the $LiTaO_3$ crystalline phase and form Er^{3+}: $LiTaO_3$ nanocrystals. The decrease in NIR excited emission intensity and fluorescence lifetimes with progression of heat-treatment time have been attributed to the clustering of Er^{3+} ions and concentration quenching. Finally, we believe that researcher would be highly benefited with the knowledge generated in this study on the Er^{3+}:$LiTaO_3$ transparent nano glass-ceramics, which could be used in the development of new efficient fiber lasers and amplifiers.

Acknowledgements

This research work was supported by BRNS/DAE under the sanction No. 2007/34/05-BRNS. The authors thank Dr. H. S. Maiti, Director, CGCRI for his keen interest and kind permission to publish this paper. Electron Microscope and X-Ray Divisions of CGCRI are also thankfully acknowledged.

References

1. W. P. Risk, T. R. Gosnell, and A. V. Nurmikko, *Compact Blue-Green Lasers*, Cambridge University Press, Cambridge, p.110, 2003.
2. International Centre for Diffraction Data, JCPDS card file no. 29-0836.
3. A. J. Moses, *The Practicing Scientist's Handbook*, Van Nostrand Reinhold Company, New York, p. 558, 1978.
4. B. Naranjo, J. K. Gimzewski, and S. Putterman, "Observation of Nuclear Fusion Driven by a Pyroelectric Crystal," *Nature*, 434 1115-1117 (2005).
5. K. S. Abedin, T. Tsuritani, M. Sato, and H. Ito, "Integrated Intracavity Quasi-Phase-Matched Second Harmonic Generation Based on Periodically Polled Nd:$LiTaO_3$," *Appl. Phys. Lett.,* 70 [1] 10-12 (1997).
6. S. Zhu, Y. Zhu, Z. Yang, H. Wang, Z. Zhang, J. Hong, C. Ge, and N. Ming, "Second-Harmonic Generation of Blue Light in Bulk Periodically Poled $LiTaO_3$," *Appl. Phys. Lett.,* 67 [3] 320-322 (1995).
7. K. Mizuuchi and K. Yamamoto, "Harmonic Blue Light Generation in Bulk Periodically Poled $LiTaO_3$," *Appl. Phys. Lett.,* 66 [22] 2943-2945 (1995).
8. H. Jain, "Transparent Ferroelectric Glass-Ceramics," *Ferroelectrics,* 306 111-127 (2004).
9. W. R. Romanowski, I. Sokólska, G. D. Dzik, and S. Gołab, "Investigation of $LiXO_3$ (X=Nb, Ta) Crystals Doped with Luminescent Ions: Recent Results," *J. Alloy Compd.*, 300-301 152-157 (2000).
10. H. Hase, H. Nasu, A. Mito, T. Hashimoto, J. Matsuoka, and K. Kamiya, "Second Harmonic Generation from Surface Crystallized Li_2O-Ta_2O_5-SiO_2 Glass," *Jpn. J. Appl. Phys.,* 35 [10] 5355-5356 (1996).

11. A. Tarafder, K. Annapurna, R. S. Chaliha, V. S. Tiwari, P. K. Gupta, and B. Karmakar, "Processing and Properties of Eu^{3+}:$LiTaO_3$ Transparent Glass-Ceramic Nanocomposites," *J. Am. Ceram. Soc.,* 92 [9] 1934-1939 (2009).
12. A. Tarafder, K. Annapurna, R. S. Chaliha, V. S. Tiwari, P. K. Gupta, and B. Karmakar, "Nanostructuring and Fluorescence Properties of Eu^{3+}:$LiTaO_3$ in Li_2O-Ta_2O_5-SiO_2-Al_2O_3 Glass-Ceramics," *J. Mater. Sci.,* 44 [16] 4495-4498 (2009).
13. T. Fujii, A. Ando, and Y. Sakabe, "Characterization of Dielectric Properties of Oxide Materials in Frequency Range from GHz to THz," *J. Eur. Ceram. Soc.,* 26 [10-11] 1857–1860 (2006).
14. M. Valant, A.-K. Axelsson, and N. Alford, "Review of Ag(Nb, Ta)O_3 as a Functional Material," *J. Eur. Ceram. Soc.,* 27 [7] 2549–2560 (2007).
15. S. Ito, T. Kokubo, and M. Tashiro, "Transparency of $LiTaO_3$-SiO_2-Al_2O_3 Glass-Ceramics in Relation to Their Microstructure," *J. Mater. Sci.,* 13 [5] 930-938 (1978).
16. Z. Yang, S. Xu, L. Hu, and Z. Jiang, "Thermal Analysis and Optical Properties of Yb^{3+}/Er^{3+}-Codoped Oxyfluoride Germanate Glasses," *J. Opt. Soc. Am. B,* 21 [5] 951-957 (2004).
17. E. Yahel and A. Hardy, "Amplified Spontaneous Emission in High-Power, Er^{3+}–Yb^{3+} Codoped Fiber Amplifiers for Wavelength-Division-Multiplexing Applications," *J. Opt. Soc. Am. B*, 20 [6] 1198-1203 (2003).
18. P. Babu, H. J. Seo, K. H. Jang, R. Balakrishnaiah, C. K. Jayasankar, K. S. Lim, and V. Lavín, "Optical Spectroscopy, 1.5μm Emission, and Upconversion Properties of Er^{3+}-Doped Metaphosphate Laser Glasses," *J. Opt. Soc. Am. B,* 24 [9] 2218-2228 (2007).

19. Y. Liu, Y. Chen, Y. Lin, Q. Tan, Z. Luo, and Y. Huang, "Energy Transfer in Yb^{3+}-Er^{3+}-Codoped Bismuth Borate Glasses," *J. Opt. Soc. Am. B*, 24 [5] 1046-1052 (2007).
20. S. Tanabe, S. Yoshii, K. Hirao, and N. Soga, "Upconversion Properties, Multiphonon Relaxation, and Local Environment of Rare-Earth Ions in Fluorophosphates Glasses," *Phys. Rev. B,* 45 [9] 4620-4625 (1992).
21. S. Tanabe, "Optical Transitions of Rare Earth Ions for Amplifiers: How the Local Structure Works in Glass," *J. Non-Cryst. Solids,* 259 1-9 (1999).
22. J. Yang, L. Zhang, L. Wen, S. Dai, L. Hu, and Z. Jiang, "Optical Transitions and Upconversion Luminescence of Er^{3+}/Yb^{3+}-Codoped Halide Modified Tellurite Glasses," *J. Appl. Phys.*, 95 [6] 3020-3026 (2004).
23. R. Balda, A. Oleaga, J. Fernández, and J.M. Fdez-Navarro, "Spectroscopy and Frequency Upconversion of Er^{3+} Ions in Lead Niobium Germanate Glasses," *Opt. Mater.,* 24 [1-2] 83-90 (2003).
24. R. R. Reddy, Y. N. Ahammed, P. A. Azeem, K. R. Gopal, T. V. R. Rao, S. Buddhudu, and N. S. Hussain, "Absoption and Emission Spectral Studies of Sm^{3+} and Dy^{3+} Doped Alkali Fluoroborate Glasses," *J. Quant. Spectrosc. Ra.*, 77 [2] 149-163 (2003).
25. M. B. Volf, *Chemical Approach to Glass*, Elsevier, Amsterdam, p.125, 1984.
26. M. Yamane and Y. Asahara, *Glasses for Photonics*, Cambridge University Press, Cambridge, UK, p.173, 2000.
27. C. Hirayama and D. Berg, "Dielectric Properties of Glasses in the System Nb_2O_5-Na_2O-SiO_2," *J. Am. Ceram. Soc.*, 46 [2] 85-88 (1963).
28. *CRC Handbook of Materials Science*, Vol. III, edited by C. T. Lynch, CRC Press, Cleveland, Ohio, p.170, 1975.

29. J. Y. Hsu and R. F. Speyer, "Comparison of the Effects of Titania and Tantalum Oxide Nucleating Agents on the Crystallization of $Li_2O \cdot Al_2O_3 \cdot 6SiO_2$ Glasses," *J. Am. Ceram. Soc.,* 72 [12] 2334-2341 (1989).

30. B. D. Cullity, *Elements of X-Ray Diffraction*, Addison-Wesley Publishing Co., London, 2nd Edition, p. 101, 1978.

31. V. L. Burdick and D. E. Day, "Coordination of Aluminium Ions in Tricalcium Aluminate," *J. Am. Ceram. Soc.*, 50 [2] 97-101 (1967).

32. H. Ono, Y. Hosokawa, K. Shinoda, K. Koyanagi, and H. Yamaguchi, "Ta-O Phonon Peaks in Tantalum Oxide Films on Si," *Thin Solid Films*, 381 [1] 57-61 (2001).

33. J. Y. Zhang, I. W. Boyd, V. Dusastre, and D. E. Williams, "Ultraviolet Annealing of Tantalum Oxide Films Grown by Photo-Induced Chemical Vapor Deposition," *J. Phys. D: Appl. Phys.*, 32 [19] L91-95 (1999).

34. A. J. Moulson and J. M. Herbert, *Electroceramics: Materials. Properties. Applications*, Chapman & Hall, London, p.222, 1990.

35. I. A. Blech, *Properties of Materials in Electronics Engineering Handbook,* 2nd Edition, D. G. Fink, D. Christiansen Ed., McGraw-Hill, New York, p. 6-30, 1986.

36. W. P. Risk, T. R. Gosnell, and A. V. Nurmikko, *Compact Blue-Green Lasers*, Cambridge University Press, Cambridge, p. 21, 2003.

37. D. E. Vernacotola, "Alkali Niobium and Tantalum Silicate Glasses and Ferroelectric Glass-Ceramics," *Key Engg. Mater.*, 94-95 379-408 (1994).

38. W. T. Carnall, P. R. Fields, and K. Rajnak, "Electronic Energy Levels in the Trivalent Lanthanide Aquo Ions. I. Pr^{3+}, Nd^{3+}, Pm^{3+}, Sm^{3+}, Dy^{3+}, Ho^{3+}, Er^{3+}, and Tm^{3+}," *J. Chem. Phys.,* 49 [10] 4424-4442 (1968).

39. G. H. Beall and D. A. Duke, *Glass-Ceramic Technology in Glass Science and Technology,* Vol. 1, Uhlmann, D. R., and Kreidl, N. J. (Eds.), Academic Press, New York, p. 403, 1983.

40. G. H. Beall and D. A. Duke, "Transparent Glass-Ceramics," *J. Mater. Sci.,* 4 [4] 340-352 (1969).

41. H. C. Van De Hulst, *Light Scattering by Small Particles,* Wiley, New York, 1957.

42. M. Mortier, A. Monteville, G. Patriarche, G. Mazé, and F. Auzel, "New Progress in Transparent Rare-Earth Doped Glass-Ceramics," *Opt. Mater.,* 16 255-267 (2001).

43. P. Riello, S. Bucella, L. Zamengo, U. Anselmi-Tamburini, R. Francini, S. Pietrantoni, and Z. A. Munir, "Erbium-Doped LAS Glass Ceramics Prepared by Spark Plasma Sintering (SPS)," *J. Eur. Ceram. Soc.,* 26 [15] 3301-3306 (2006).

44. M. J. Dejneka, "The Luminescence and Structure of Novel Transparent Oxyfluoride Glass-Ceramics," *J. Non-Cryst. Solids*, 239 [1-3] 149-155 (1998).

45. K. Pátek, *Glass Lasers*, Butterworth & Co (Publishers) Ltd., London, p.95, 1970.

46. J. H. Campbell and T. I. Suratwala, "Nd-Doped Phosphate Glasses for High-Energy/High-Peak-Power Lasers," *J. Non-Cryst. Solids*, 263-264 318-341 (2000).

47. U. Kang, A. A. Zhilin, D. P. Logvinov, A. A. Onushchenko, V. A. Savost'yanov, T. I. Chuvaeva, and A. V. Shashkin, "Transparent Nd^{3+}-Activated Glass-Ceramics in the Li_2O-Al_2O_3-SiO_2 System: Physicochemical Aspects of Their Preparation and Optical Characteristics," *Glass Phys. Chem.,* 27 [4] 344-352 (2001).

FIGURE CAPTIONS

Fig.1. DTA curve of precursor powdered glass.

Fig. 2. (Color online) Photograph of precursor glass and nano glass-ceramics (thickness: 2 mm) laid over the writing to show their transparency.

Fig. 3. Variation of refractive indices (Cauchy fitted) of (a) precursor glass and (d) 10 h heat-treated nano glass-ceramics as a function of wavelength.

Fig. 4. XRD patterns of the samples (a)-(g).

Fig. 5. Variation of crystal sizes as a function of heat-treatment time.

Fig. 6. FESEM images of samples **(a)** c and **(b)** f.

Fig. 7. (a) TEM image and SAED (Inset) and (b) HRTEM lattice fringes $LiTaO_3$ nanocrystals of sample (c).

Fig. 8. FT-IRR Spectra of (a) precursor glass, (b) 3 h and (g) 100 h heat-treated samples.

Fig. 9. Variation of dielectric constant of precursor glass and nano glass-ceramics as a function of heat-treatment time.

Fig. 10. Absorption spectra of samples (a)-(c) (thickness: 2 mm). Inset shows the hypersensitive transition ($^4I_{15/2} \leftrightarrow {}^2H_{11/2}$) spectral profile of Er^{3+} ions in samples (a)-(c) at wavelength ranges 510-535 nm (a. u. = absorbance unit).

Fig. 11. UV-excited fluorescence spectra (λ_{ex} = 378 nm) of Er^{3+}-doped precursor glass and samples heat-treated for various duration.

Fig. 12. (Color online) Excitation spectra (λ_{em} = 549 nm) of precursor glass (a) and 5 h heat-treated sample (c).

Fig. 13. (Color online) Fluorescence spectra (λ_{ex} = 984 nm) around 1570 nm of Er^{3+}-doped samples precursor glass (a) and (b, c and g) heat-treated for various duration.

Fig. 14. (Color online) Decay curves for the $^4I_{13/2} \rightarrow {}^4I_{15/2}$ transition at1570 nm under excitation at 984 nm of samples (a)-(c), (e) and (f).

Table I. Some Measured and Calculated Properties of Er^{3+}:Li_2O-Ta_2O_5-SiO_2-Al_2O_3 Precursor Glass

Properties	**Corresponding Value**
Average molecular weight, M_{av}	142.41
Density, ρ ($g.cm^{-3}$)	4.739
Refractive indces:	
n_F (at 486.1 nm)	1.8050
n_D (at 589.2 nm)	1.7891
n_C (at 656.3 nm)	1.7819
Dispersive power ($1/\upsilon_D$)	0.029
Molar refractivity, R_M (cm^3)	12.72
Electronic polarizability, α (cm^3)	1.93×10^{-21}
Er^{3+} ion concentration, $N_{Er^{3+}}$ (ions/cm^3)	5.24×10^{19}
Er^{3+}-Er^{3+} inter ionic distance, R_i (Å)	27
Glass transition temperature, T_g (^oC)	698
Crystallization peak, T_p (^oC)	820

Figures

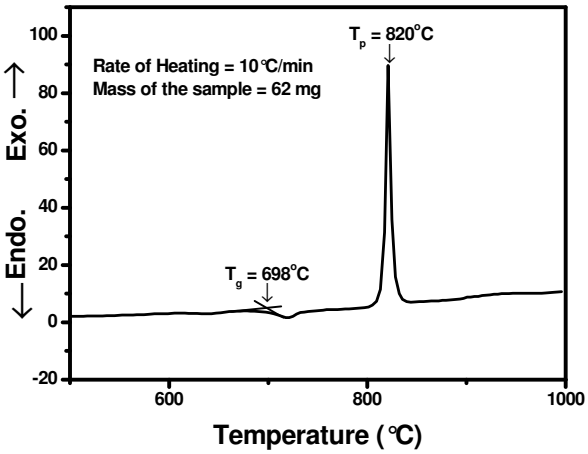

Fig. 1. DTA curve of precursor powdered glass.

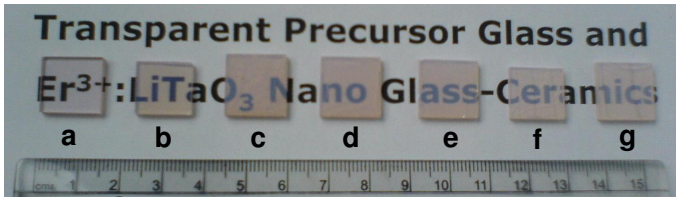

Fig. 2. (Color online) Photograph of precursor glass and nano glass-ceramics (thickness: 2 mm) laid over the writing to show their transparency.

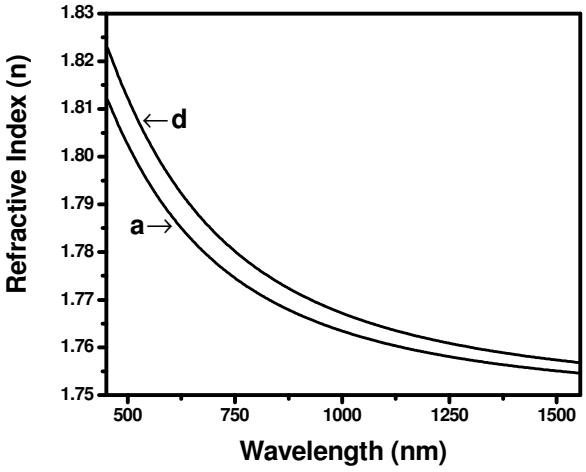

Fig. 3. Variation of refractive indices (Cauchy fitted) of (a) precursor glass and (d) 10 h heat-treated nano glass-ceramics as a function of wavelength.

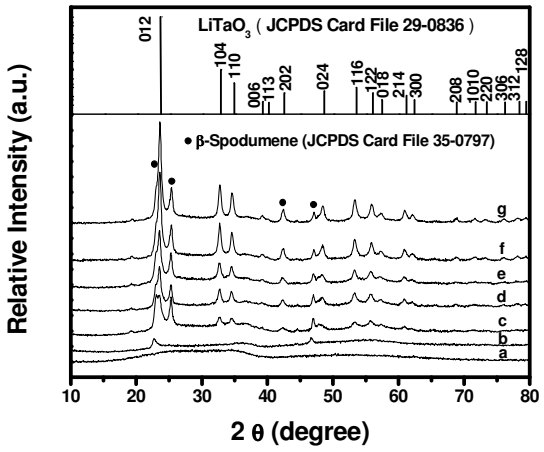

Fig. 4. XRD patterns of the samples (a)-(g).

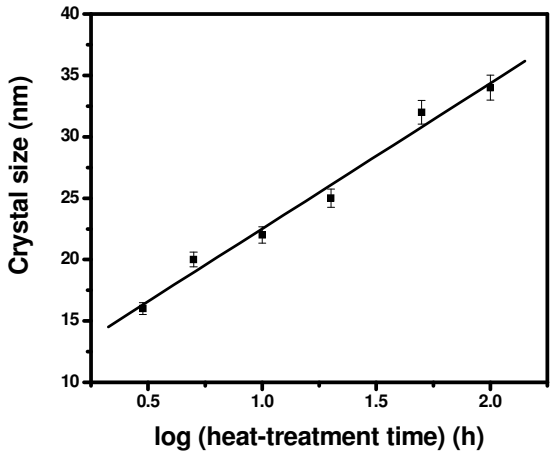

Fig. 5. Variation of crystal sizes as a function of heat-treatment time.

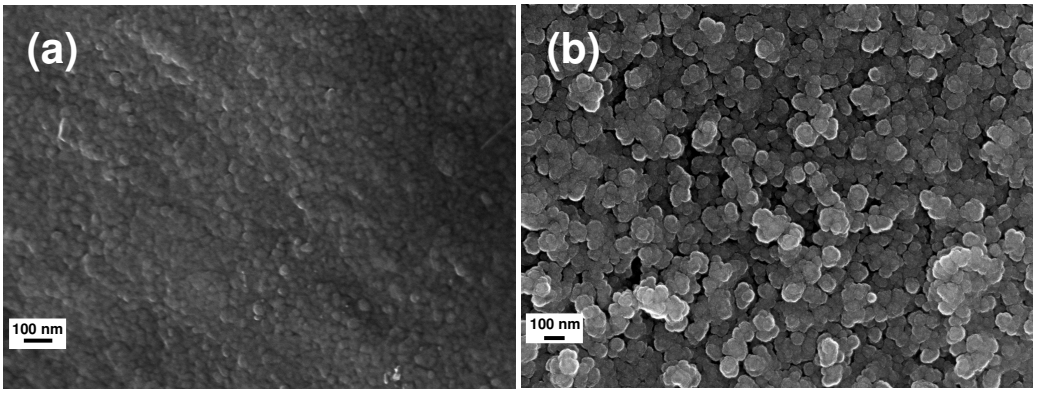

Fig. 6. FE-SEM images of samples (a) c and (b) f.

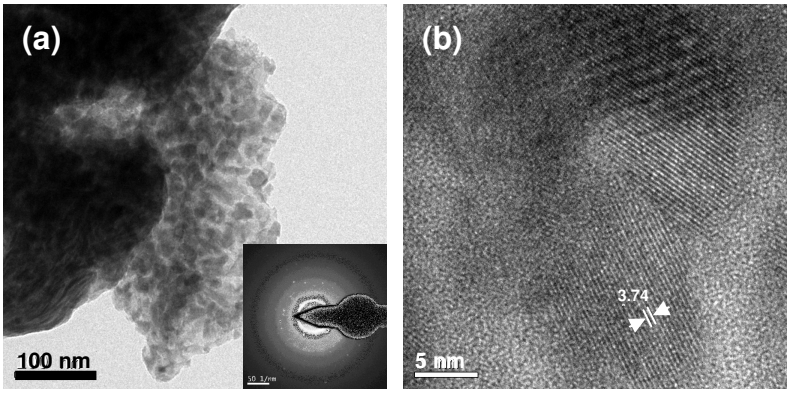

Fig. 7. (a) TEM image and SAED (Inset) and (b) HRTEM lattice fringes of $LiTaO_3$ nanocrystals of sample (c).

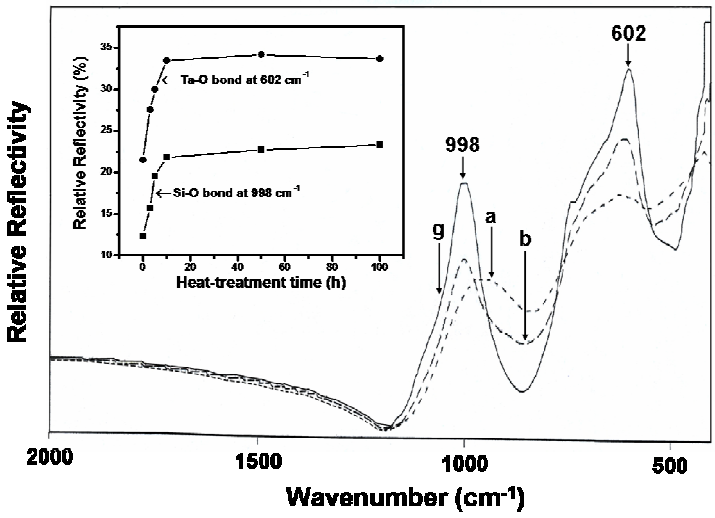

Fig. 8. FT-IRR Spectra of (a) precursor glass, (b) 3 h and (g) 100 h heat-treated samples.

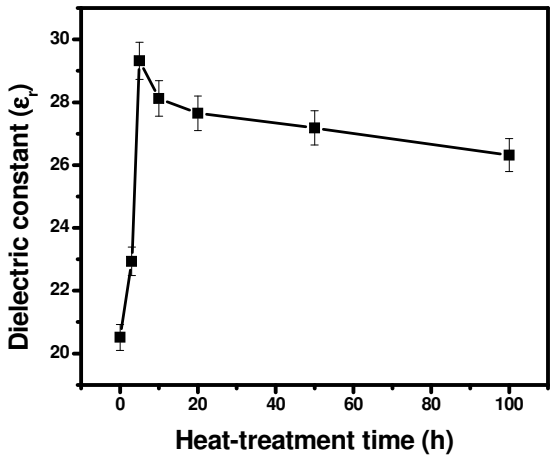

Fig.9. Variation of dielectric constant of precursor glass and nano glass-ceramics as a function of heat-treatment time.

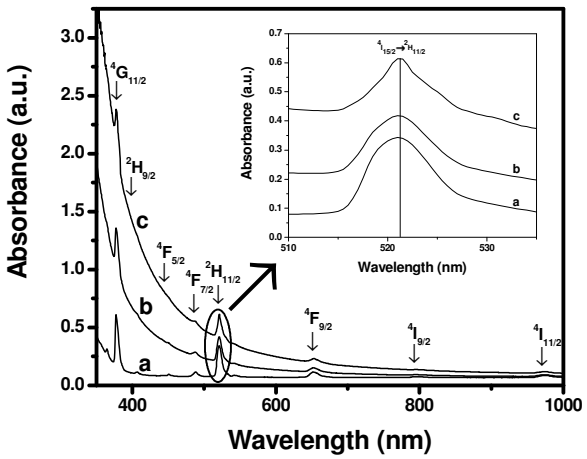

Fig. 10. Absorption spectra of samples (a)-(c) (thickness: 2 mm). Inset shows the hypersensitive transition ($^4I_{15/2} \leftrightarrow {}^2H_{11/2}$) spectral profile of Er^{3+} ions in samples (a)-(c) at wavelength ranges 510-535 nm (a. u. = absorbance unit).

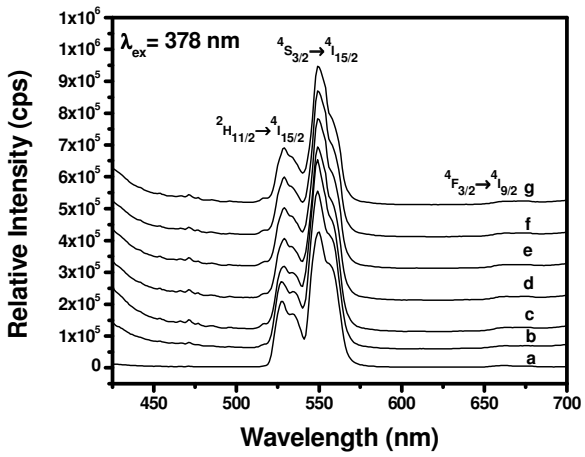

Fig. 11. UV-excited fluorescence spectra (λ_{ex} = 378 nm) of Er^{3+}-doped precursor glass and samples heat-treated for various duration.

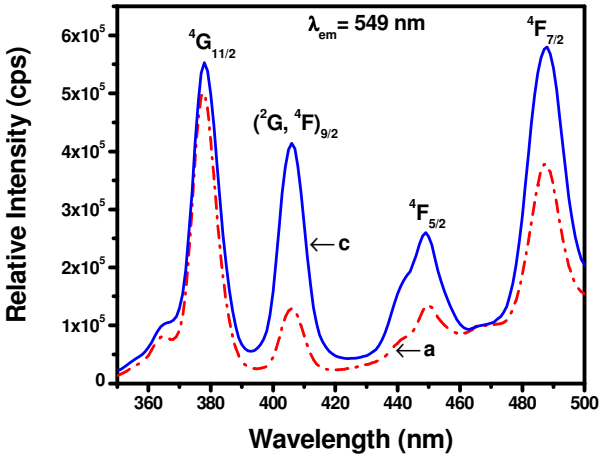

Fig. 12. (Color online) Excitation spectra (λ_{em} = 549 nm) of precursor glass (a) and 5 h heat-treated sample (c).

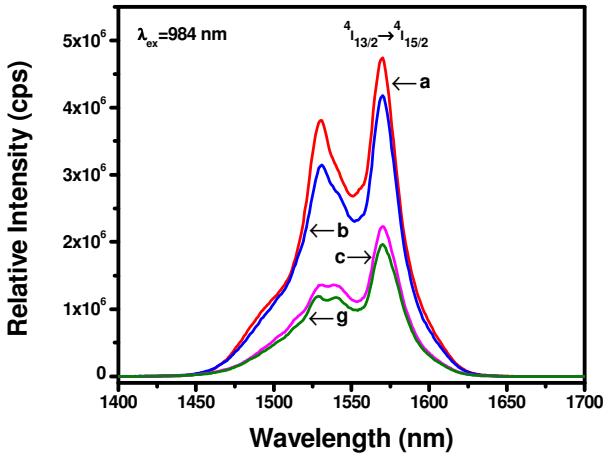

Fig. 13. (Color online) Fluorescence spectra (λ_{ex} = 984 nm) around 1570 nm of Er^{3+}-doped samples precursor glass (a) and (b, c and g) heat-treated for various duration.

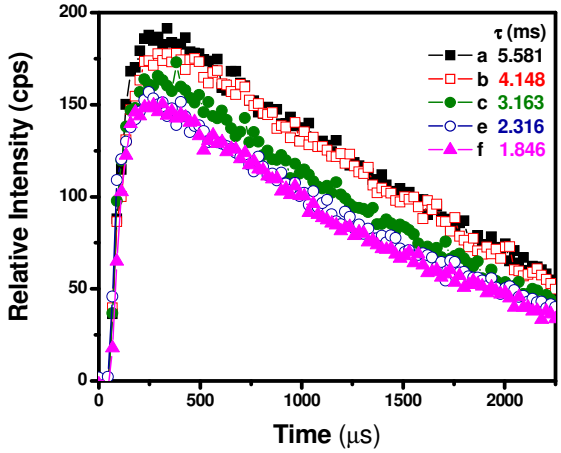

Fig. 14. (Color online) Decay curves for the $^4I_{13/2} \rightarrow {}^4I_{15/2}$ transition at1570 nm under excitation at 984 nm of samples (a)-(c), (e) and (f).